Thermal decomposition of methanethiol and ethanethiol

ARTICLE *in* THE JOURNAL OF PHYSICAL CHEMISTRY · JULY 1987

Impact Factor: 2.78 · DOI: 10.1021/j100299a040

Thermal Decomposition of Methanethiol and Ethanethiol

Kim K. Baldridge,* Mark S. Gordon,* and Douglas E. Johnson

Department of Chemistry, North Dakota State University, Fargo, North Dakota 58105
(Received: December 29, 1986)

Selected ground-state decomposition pathways for methanethiol and ethanethiol are considered, using ab initio electronic structure calculations including electron correlation. The decomposition of methanethiol to form methylene and hydrogen sulfide requires a large activation energy (108.3 kcal/mol). In contrast, the energy required for the homolytic cleavage of the C–S bond is calculated to be just 67.2 kcal/mol. For ethanethiol, carbene formation is more competitive with radical processes. Here, the activation energy for the 1,1 elimination of H_2S to form ethylidene (76.9 kcal/mol) is smaller than that for the direct formation of ethylene via a 1,2 elimination (106.6 kcal/mol) and only 12 kcal/mol greater than the calculated C–S bond enthalpy (65.1 kcal/mol). A static pyrolysis mechanism was also considered as one of the three radical processes and found to be less favorable energetically. All calculations were performed at the MP4/6-31G(d,p) level, using SCF/6-31G(d,p) geometries. The effect of triple substitutions in the MP4 calculations was found to be on the order of 3 kcal/mol for the molecular decomposition of methanethiol.

Proem

The pyrolysis chemistry of alkanethiols has been examined sporadically since the initial report of ethanethiol pyrolysis by Sabatier and Mailhe in 1910.[1] The thermal chemistry of methanethiol,[2] ethanethiol,[2-4] 1- and 2-butanethiols,[5] 1-pentanethiol,[6,7] 2-methyl-2-propanethiol,[5,8,9] bicyclo[2.2.1]heptane-2-thiols,[10] and phenylmethanethiol[2] has been examined in the intervening years. Most investigations have been solely kinetic examinations of the disappearance of the initial thiol with limited attention paid to complete characterization of reaction products. An understanding of the reaction mechanism has been hindered by disagreement on the identity of the initial pyrolysis products. Alkenes are now believed to be the primary pyrolysis reaction products, although the reaction mixture is frequently complicated by the presence of elemental sulfur, sulfides, disulfides, and lower molecular weight hydrocarbons.[2,7,11] The problem is further complicated by the dependence of the product mixture on reaction conditions and structure of the initial thiol.[12] As an initial attempt to unravel some of the experimental uncertainties, this paper presents the results of a theoretical investigation of the energetics and transition-state structures for unimolecular decomposition reactions of methanethiol and ethanethiol.

Two radical reaction mechanisms have been proposed to account for the product distributions and observed reaction kinetics of alkanethiol pyrolysis.[2,5] The simplest radical mechanism involves homolytic cleavage of the carbon–sulfur bond, yielding alkyl and thiyl radicals, followed by hydrogen abstraction from the alkyl radical by the thiyl radical:

$$RCH_2CH_2SH \rightarrow RCH_2CH_2^{\bullet} + {}^{\bullet}SH \quad (1a)$$

$$RCH_2CH_2^{\bullet} + {}^{\bullet}SH \rightarrow RCH{=}CH_2 + H_2S \quad (1b)$$

This mechanism neatly accounts for the formation of an alkene from a primary thiol and can explain the first-order reaction kinetcs observed in flow and static pyrolyses. However, a more complicated radical chain mechanism has recently been proposed[5] in which carbon–sulfur bond homolysis (eq 1a) is followed by hydrogen atom abstraction by a thiyl radical from another molecule of thiol to yield a mercaptoalkyl radical (eq 2a). Fragmentation of the mercaptoalkyl radical yields an alkene and the chain-carrying thiyl radical:

$$RCH_2CH_2SH + {}^{\bullet}SH \rightarrow R\dot{C}HCH_2SH + H_2S \quad (2a)$$

$$R\dot{C}HCH_2SH \rightarrow RCH{=}CH_2 + {}^{\bullet}SH \quad (2b)$$

This "static pyrolysis" mechanism is the microscopic reverse of the mechanism for the radical addition of a thiol to an alkene and accounts for the reaction products and kinetic order observed in the static pyrolysis.[13]

Several unimolecular reaction mechanisms have been proposed to account for the products and kinetic orders observed in alkanethiol pyrolyses. The simplest mechanism is a concerted 1,2 elimination of hydrogen sulfide from the thiol to form the alkene:[2]

$$RCH_2CH_2SH \rightarrow RCH{=}CH_2 + H_2S \quad (3)$$

Alternatively, 1,1 elimination of hydrogen sulfide from 1-pentanethiol has been proposed by Thompson, Meyer, and Ball to account for the reactivity differences between primary and tertiary alkanethiols:[7]

$$RCH_2CH_2SH \rightarrow H_2S + [RCH_2CH] \rightarrow RCH{=}CH_2 \quad (4)$$

A carbene intermediate was identified in the pyrolysis of the isomeric bicyclo[2.2.1]heptane-2-thiols.[10]

Other possibilities include formation of a thioaldehyde

$$RCH_2CH_2SH \rightarrow H_2 + RCH_2C(S)H \quad (5)$$

cleavage of a carbon–carbon bond

$$RCH_2CH_2SH \rightarrow {}^{\bullet}CH_2R + {}^{\bullet}CH_2SH \quad (6a)$$

and 1,1 elimination of dihydrogen from the mercapto-bearing carbons of primary thiols

$$RCH_2CH_2SH \rightarrow RCH_2CSH + H_2 \quad (6b)$$

In view of the foregoing discussion, we will consider in this work the relative energetics for decomposition reactions of the type 1–6 for the methanethiol and ethanethiol on their closed-shell ground-state surfaces. The decomposition pathways to be considered for methanethiol are

(1) Sabatier, S.; Mailhe, C. R. *C. R. Acad. Sci.* **1910**, *150*, 1571.
(2) Sehon, A. H.; Darwent, B. deB. *J. Am. Chem. Soc.* **1954**, *76*, 4806.
(3) Trenner, N. R.; Taylor, H. A. *J. Chem. Phys.* **1933**, *1*, 77.
(4) Boivin, J. L.; MacDonald, R. *Can. J. Chem.* **1955**, *33*, 1281.
(5) Bamkole, T. O. *J. Chem. Soc., Perkin Trans. 2* **1977**, 439.
(6) Malisoff, W. M.; Marks, E. M. *Ind. Eng. Chem.* **1931**, *23*, 1114.
(7) Thompson, C. J.; Meyer, R. A.; Ball, J. S. *J. Am. Chem. Soc.* **1952**, *74*, 3287.
(8) Thompson, C. J.; Meyer, R. A.; Ball, J. S. *J. Am. Chem. Soc.* **1952**, *74*, 3284.
(9) Tsang, W. *J. Chem. Phys.* **1964**, *40*, 1498.
(10) Johnson, D. E.; Dimian, A. F. *J. Chem. Soc., Chem. Commun.*, in press.
(11) Faragher, W. F.; Morrell, J. C.; Comay, S. *Ind. Eng. Chem.* **1928**, *20*, 527.
(12) For example, 2-methyl-2-propanethiol has been examined in flow,[8] shock tube,[9] and static[5] pyrolysis. Each investigation proposed a different mechanism.
(13) Pryor, W. A. *Mechanisms of Sulfur Reactions*; McGrall-Hill: New York, 1962; p 75.

0022-3654/87/2091-4145$01.50/0

$$CH_3SH \rightarrow :CH_2 + H_2S \quad (7a)$$

$$CH_3SH \rightarrow {}^{\bullet}CH_3 + SH \quad (7b)$$

$$CH_3SH \rightarrow :CHSH + H_2 \quad (7c)$$

$$CH_3SH \rightarrow H_2CS + H_2 \quad (7d)$$

It has been observed experimentally that methanethiol primarily decomposes by a complicated free radical mechanism.[2] The activation energy for the C–S bond dissociation at 298 K is 72.4 kcal/mol.[14]

Seven decomposition pathways for ethanethiol are considered. These include four molecular eliminations (8a, 8b, 8c, 8d), two simple homolytic cleavages (8e and 8f), and one complex radical process (8g). The last reaction sequence (8g) is the analogue of a static pyrolysis mechanism (2).

$$CH_3CH_2SH \rightarrow CH_2{=}CH_2 + H_2S \quad (8a)$$

$$CH_3CH_2SH \rightarrow :CHCH_3 + H_2S \quad (8b)$$

$$CH_3CH_2SH \rightarrow :CHCH_2SH + H_2 \quad (8c)$$

$$CH_3CH_2SH \rightarrow CH_3CSH + H_2 \quad (8d)$$

$$CH_3CH_2SH \rightarrow CH_3CH_2^{\bullet} + {}^{\bullet}SH \quad (8e)$$

$$CH_3CH_2SH \rightarrow {}^{\bullet}CH_3 + {}^{\bullet}CH_2SH \quad (8f)$$

$$CH_3CH_2SH \rightarrow CH_3CH_2^{\bullet} + {}^{\bullet}SH$$

$$HS^{\bullet} + CH_3CH_2SH \rightarrow H_2S + {}^{\bullet}CH_2CH_2SH \quad (8g)$$

$${}^{\bullet}CH_2CH_2SH \rightarrow CH_2{=}CH_2 + {}^{\bullet}SH$$

Experimentally, ethanethiol is observed to decompose principally by *inter*molecular elimination to yield ethylene and hydrogen sulfide and by the cleavage of the C–S bond to give ethyl and hydrosulfide radicals.[2] The latter process requires only 69.1 kcal/mol.[14]

Theoretical Methods

All molecular structures, including those for transition states in reactions 7a, 7b, 8a, and 8b, were determined by the search methods in GAUSSIAN82.[15] These geometry calculations were performed at the SCF level with the 3-21G*,[16] 6-31G(d),[17] and 6-31G(d,p)[18] basis sets. Unrestricted Hartree–Fock (UHF) calculations were performed for all radical species. In all such cases, the expectation value of the spin squared operator, $\langle S^2 \rangle$, was between 0.75 (the exact value) and 0.77; thus there is little contamination from higher spin states. The minimal STO-2G*[19] basis set was used to provide initial guesses for saddle points. Although only 6-31G(d,p) structures will be quoted here, it is important to note that most structural features at both minima and saddle points differ only in detail from those calculated at the STO-2G* level. The transition states were verified by diagonalizing the saddle point force constant matrices. At each of the final 6-31G(d,p) structures, single point calculations were carried out with fourth-order many-body perturbation theory (MP4),[20,21] denoted MP4/6-31G(d,p)//6-31G(d,p). The effect of triple substitutions on calculated energy differences was determined from the MP4(SDTQ)/6-31G(d,p) calculations on reactions 7a, 7b, 7c, and 7d. Only MP4(SDQ)/6-31G(d,p) calculations were performed for the reactions involving larger molecules. To facilitate direct comparisons between theory and

TABLE I: Calculated and Experimental Equilibrium Geometries[a]

molecule	point group	geometrical parameter	6-31G(d,p)	expt
$^1CH_2$	C_{2v}	r(CH)	1.099	1.111[b]
		∠(HCH)	102.9	102.4
H_2	$D_{\infty h}$	r(HH)	0.733	0.741[c]
H_2S	C_{2v}	r(SH)	1.327	1.336[b]
		∠(HSH)	94.4	92.1
C_2H_4	D_{2h}	r(CC)	1.316	1.335[d]
		r(CH)	1.076	1.081
		∠(CCH)	121.7	121.3
CH_3SH	C_s	r(CS)	1.817	1.819[b]
		r(SH)	1.327	1.336
		$r(CH_{tr})$	1.082	1.091
		$r(CH_q)$	1.081	1.091
		$\angle(SCH_{tr})$	106.6	
		∠(HCSH)	61.6	
		∠(CSH)	98.0	96.5
		∠(HCH)		109.8
CH_3CH_2SH	C_s	r(CC)	1.525	
		r(CS)	1.828	
		r(SH)	1.327	
		∠(HSC)	98.1	
		∠(SCC)	109.7	
H_2CS	C_s	r(CS)	1.597	1.611[b]
		r(CH)	1.079	1.093
		∠(HCS)	122.5	
		∠(HCH)	115.0	116.9
$^{\bullet}SH$	$C_{\infty v}$	r(SH)	1.3309	1.341[e]
$^{\bullet}CH_3$	C_s	r(HC)	1.073	1.079[c]
		∠(HCH)	120.0	120.0
:CHSH	C_s	r(CS)	1.674	
		r(HS)	1.330	
		r(HC)	1.092	
		∠(HSC)	100.6	
		∠(HCS)	104.2	
$^{\bullet}CH_2SH$	C_1	r(CS)	1.748	
		r(HS)	1.326	
		r(HC)	1.073	
		∠(HCS1)	116.0	
		∠(HCS2)	120.3	
		∠(HSC)	98.3	
		∠(HSCH)	183.4	
		∠(HCSH)	26.2	
$^{\bullet}CH_2CH_3$	C_s	r(HC)	1.091	
		r(CC)	1.497	
		∠(CCH)	111.7	
		∠(HCCH)	82.2	
$^{\bullet}CH_2CH_2SH$	C_s	r(CC)	1.491	
		r(CS)	1.843	
		r(HS)	1.329	
		∠(SCC)	110.1	
		∠(HSC)	97.8	
		∠(HCCS)	82.2	
$:CHCH_3$	C_1	r(CC)	1.482	
		r(HC)	1.088	
		∠(HCC)	117.3	
		∠(HCCH)	32.3	

[a] Bond lengths in angströms, angles in degrees. [b] Calloman, J. H.; Hirota, E.; Kuchitsu, K.; Lafferty, W. J.; Maki, A. G.; Pote, C. S. *Structure Data on Free Polyatomic Molecules*, Landolt-Bornstein, New Series, Group II, Vol. 7, Hellwege, K. H., Hellwege, A. M., Eds.; Springer-Verlag, Berlin. [c] Binkely, J. S.; Pople, J. A.; Hehre, W. J. *J. Am. Chem. Soc.* **1980**, *102*, 939. [d] Duncan, J. L. *Mol. Phys.* **1974**, *28*, 1177. [e] Herzberg, G.; Huber, K. D. *Molecular Spectra and Molecular Structure. 4. Constants of Diatomic Molecules*; Van Nostrand: Princeton, NJ, 1979. [f] Sana, M.; Leroy, G.; Villaueces, J. L. *Theoret. Chim. Acta* **1984**, *65*, 109.

(14) Wagman, D. D.; Evans, W. J.; Parker, V. B.; Schumm, R. H.; Halow, I.; Bailey, S. M.; Churney, K. L.; Nuttal, R. L. *J. Phys. Chem. Ref. Data* **1982**, *11*, Suppl. No. 2.

(15) Binkley, J. S.; Frisch, M. J.; DeFrees, D. J.; Krishnan, R.; Whiteside, R. A.; Schlegel, H. B.; Fluder, E. M.; Pople, J. A. GAUSSIAN82, Carnegie-Mellon University, Pittsburgh, PA, 1983.

(16) Pietro, W. J.; Francl, M. M.; Hehre, W. J.; DeFrees, D. J.; Pople, J. A.; Binkley, J. S. *J. Am. Chem. Soc.* **1982**, *104*, 5039.

(17) Gordon, M. S. *Chem. Phys. Lett.* **1980**, *76*, 163.

(18) Hariharan, P. C.; Pople, J. A. *Theor. Chim. Acta* **1973**, *28*, 213.

(19) Hehre, W. J.; Stewart, R. F.; Pople, J. A. *J. Chem. Phys.* **1969**, *51*, 2657.

(20) (a) Binkley, J. S.; Pople, J. A. *Int. J. Quantum Chem.* **1975**, *9*, 229. (b) Pople, J. A.; Binkley, J. S.; Krishnan, R. *Int. J. Quantum Chem. Symp.* **1976**, *10*, 1.

(21) Krishnan, R.; Frisch, M. J.; Pople, J. A. *J. Chem. Phys.* **1980**, *72*, 4244.

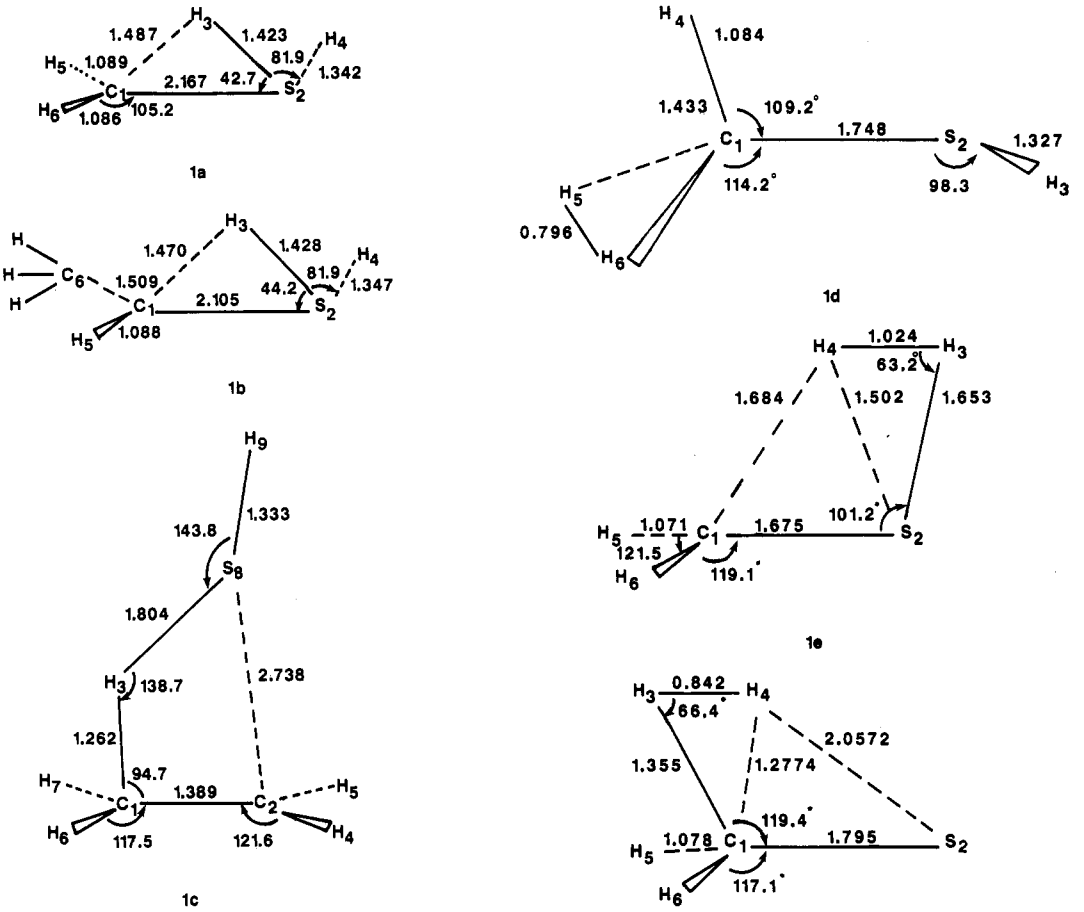

Figure 1. 6-31G(d,p) transition-state structures. Bond lengths in Å, angles in degrees. Angles ($\angle$) and dihedral angles (d) for these structures are as follows: 1a. Reaction 7a: $d(5123) = 47.3$, $d(6123) = -70.6$, $d(4231) = 199.6$; $\angle(512) = 106.6$, $\angle(612) = 105.2$. 1b. Reaction 8b: $d(5123) = 45.0$, $d(6123) = -82.8$, $d(4231) = 206.2$; $\angle(512) = 106.7$, $\angle(612) = 113.7$. 1c. Reaction 8a: $d(4321 = 5321) = 89.1$, $d(6231 = 7231) = 107.0$; $\angle(428 = 528) = 71.8$. 1d. Reaction 7c: $d(6123) = 83.9$, $d(4123) = 196.1$. 1e. Reaction 7d; higher energy transition state: $d(4321) = 0.0$, $d(5123 = 6123) = 93.1$; $\angle(143) = 142.4$, $\angle(614) = 109.3$. 1f. Reaction 7d; lower energy transition state: $d(4321) = 0.0$, $d(5123) = 109.5$; $\angle(513) = 92.0$.

experiment, experimental energy differences were converted to 0 K by using the approach described previously,[22,23] scaling the SCF/6-31G(d,p) calculated frequencies by a factor of 0.89.

Using a modified version of GAMESS,[24] we generated the intrinsic reaction coordinate (IRC)[25] connecting the reactants, the transition state, and products for several of the reactions considered. The IRC is the steepest descent path connecting the transition state to both reactants and products. SCF/STO-2G* IRC's were generated for reactions 7a, 7c, 7d, and 8b, and an SCF/6-31G(d) IRC was obtained for reaction 8a.

Using the spline fitting program XYPLOT,[26] we generated a linear least motion (LLM) path connecting reactants with a complex found on the methanethiol potential energy surface. The LLM path consists of a series of SCF/6-31G(d,p) single point energies at ten equally spaced intervals from reactants to complex.

Results and Discussion

A. Molecular Geometries. The 6-31G(d,p) geometries of the stable molecules and reactive intermediates considered in this work are given in Table I. The structures of the known compounds are seen to be in good agreement with the experimental values. Notice the shortening of the C–S bond length along the series: CH_3SH, CH_2SH, CHSH. Successive removal of hydrogen from carbon increases the possibility of C–S π bonding, thereby shortening the C–S bond length.

TABLE II: CS Bond Lengths for Methanethiol Complexes 4a and 4b, Methanethiol, and Thiolformaldehyde

molecule	SCF/6-31G(d,p) C–S bond length, Å
CH_3SH	1.817
H_2CS	1.597
complex 4a	2.175
complex 4b	1.662

The structures for the 6-31G(d,p) transition states for reactions 7a, 7b, and 8a are shown in Figure 1. Notice the similarity in the transition-state structure for reactions 7a and 8b. Both have C_1 symmetry, the major difference being the longer C–S bond length in the former structure. For both reactions, the transferring hydrogen is closer to the sulfur atom at the saddle point, suggesting late transition states for reactions 7a and 8b as written. The transition-state structure for the 1,2 elimination of H_2S (reaction 8a, Figure 1c) has C_s symmetry, with the sulfur moving away from the ethylene fragment much sooner than the hydrogen. The four-centered transition-state structure for this reaction is similar to that found for the reaction of HCl with ethylene.[28]

The normal mode corresponding to the imaginary frequency for the transition state of reaction 7a is illustrated in Figure 2a. The motion suggested by the normal mode is consistent with the reactants and products connected by the transition state, according

(22) Pople, J. A.; Luke, B. T.; Frisch, M. J.; Binkley, J. S. *J. Phys. Chem.* **1985**, *89*, 2198.
(23) Gordon, M. S.; Truhlar, D. G. *J. Am. Chem. Soc.*, submitted for publication.
(24) Dupuis, M.; Spangler, D.; Wendoloski, J. J. *NRCC Software Catalog* **1980**, 1, Program QG01.
(25) Schmidt, M. W.; Gordon, M. S.; Dupuis, M. *J. Am. Chem. Soc.* **1985**, *107*, 2585, and references cited therein.
(26) Schmidt, M. W. XYPLOT, unpublished.
(27) Pople, J. A.; Raghavachari, K.; Frisch, M. J.; Binkley, J. S.; Schleyer, P. R. *J. Am. Chem. Soc.* **1983**, *105*, 6389.
(28) Nagase, S.; Kudo, T. *J. Chem. Soc., Chem. Commun.* **1983**, 6, 363.

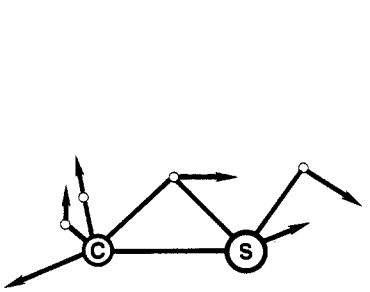

IMAGINARY FREQUENCY=778i cm^{-1}

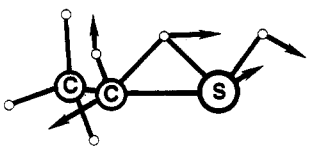

IMAGINARY FREQUENCY=973i cm^{-1}

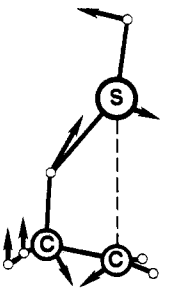

IMAGINARY FREQUENCY=1212i cm^{-1}

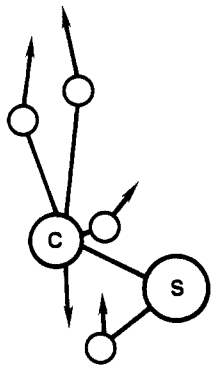

IMAGINARY FREQUENCY = 1111i cm^{-1}

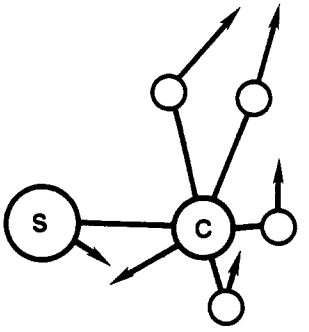

IMAGINARY FREQUENCY = 1124i cm^{-1}

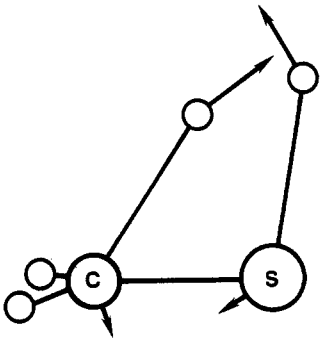

IMAGINARY FREQUENCY = 3089i cm^{-1}

Figure 2. 6-31G(d,p) normal modes corresponding to imaginary frequencies for transition states for: (a) reaction 7a, (b) reaction 8b, (c) reaction 8a, (d) reaction 7c, (e) reaction 7d (lower energy transition state), (f) reaction 7d (higher energy transition state).

TABLE III: Net Energy Differences and Energy Barriers for Methanethiol and Ethanethiol Decomposition[a]

a. Net Energy Differences

	reaction	SDQ MP2	SDQ MP3	SDQ MP4	SDQ ΔH	SDTQ MP4	SDTQ ΔH
(7a)	$CH_3SH \rightarrow :CH_2 + H_2S$	119.2	114.1	112.5		114.4	104.8
(7b)	$CH_3SH \rightarrow CH_3 + SH$	76.6	73.2	72.4		74.6	67.2
(7c)	$CH_3SH \rightarrow :CHSH + H_2$	94.6	93.5	91.2		90.0	80.4
(7d)	$CH_3SH \rightarrow H_2CS + H_2$	37.3	39.5	37.8		35.7	30.3
	$CH_3SH \rightarrow$ complex 4a	100.8	98.3	97.2		97.3	92.9
	$CH_3SH \rightarrow$ complex 4b	77.8	79.2	78.8		77.7	75.5
(8a)	$C_2H_5SH \rightarrow CH_2{=}CH_2 + H_2S$	27.6	26.2	25.1	19.3		
(8b)	$C_2H_5SH \rightarrow :CHCH_3 + H_2S$	110.1	104.6	103.2	94.6		
(8c)	$C_2H_5SH \rightarrow CH_3CH_2 + SH$	76.7	72.5	71.7	65.1		
(8f)	$C_2H_5SH \rightarrow CH_3SH + CH_2$	94.4	90.6	89.5	80.0		
(8c)	$C_2H_5SH \rightarrow CHCH_2SH + H_2$	125.7	122.4	120.8	109.0		
(8d)	$C_2H_5SH \rightarrow CH_3CSH + H_2$	90.3	89.2	87.1	73.2		
(8g)	static pyrolysis mechanism	104.3	98.5	96.7	84.4		
	$C_2H_5SH \rightarrow$ complex 4c	77.4	79.2	78.7	76.2		

b. Energy Barriers

reaction	SDQ MP2	SDQ MP3	SDQ MP4	SDQ E_a	SDTQ MP4	SDTQ E_a
$CH_3SH \rightarrow :CH_2 + H_2S$	117.3	115.4	114.5		113.8	108.3
$CH_3SH \rightarrow :CHSH + H_2$	106.8	106.1	104.7		103.6	97.8
$CH_3SH \rightarrow H_2CS + H_2$	96.7	98.2	97.8		96.6	89.0
$C_2H_5SH \rightarrow CH_2{=}CH_2 + H_2S$	82.6	84.5	82.5	76.9		
$C_2H_5SH \rightarrow :CHCH_3 + H_2S$	113.6	112.7	111.9	106.6		

[a] In units of kcal/mol. All results obtained by using the 6-31G(d,p) basis set.

to reaction 7a. To verify this we have examined the IRC for the reaction at the STO-2G* level. Schematics of the IRC are shown in Figure 3a. They clearly show that the transition structure leads smoothly to the proposed reactants and products.

Raghavachari et al.[29] predicted the existence of an addition complex between H_2S and SiH_2:

We find two such CH_2---SH_2 complexes, illustrated in Figure 4. The C–S bond lengths for these species are compared to those for C–S singly and doubly bonded species in Table II. The higher energy structure in Figure 4a corresponds to the interaction of the empty p orbital on carbon with the sulfur lone pair. The lower energy complex (Figure 4b) has a much shorter C–S bond length, closer in value to that of the doubly bonded species H_2CS. This suggests an ylide-like structure:

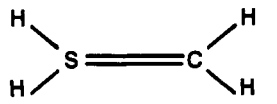

The 6-31G(d,p) Mulliken populations are consistent with this, showing a positive charge buildup on sulfur and a negative buildup on carbon, compared to the separated species:

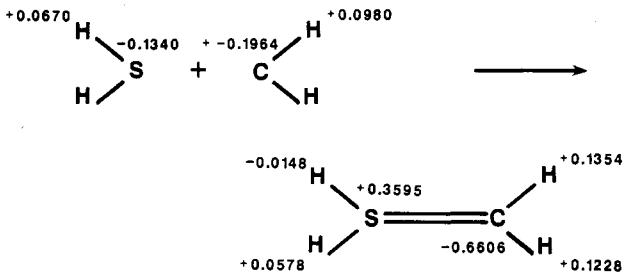

A further analysis of this lower energy complex is provided by the 6-31G(d,p) Edmiston–Ruedenberg energy-localized molecular orbitals.[30] Selected bonds and lone pairs for the lower energy complex (Figure 4b) are depicted in Figure 5. These plots are consistent with the predicted ylide-like character. Figure 5a shows the sulfur–carbon bond orbital for the structure. Analysis of the MO coefficients for this orbital indicates partial π-type character. Figure 5b shows the carbon lone pair, which is rather diffuse and is polarized toward the sulfur. The sulfur lone pair, shown in Figure 5c, has mostly s character and exhibits little back-bonding toward the carbon.

A SCF/6-31G(d,p) linear least motion path connecting the two complexes is illustrated in Figure 6a. The higher energy complex is 10.7 kcal/mol above the lower energy complex at this level of computation. The LLM path suggests that a barrier of less than 1 kcal/mol separates complex 4a from 4b. Analysis of the force field for the higher energy complex reveals two very low-frequency vibrations, one with a′ symmetry and one with a″ symmetry. The a′ vibration corresponds to the approach of the two fragments CH_2 and SH_2 (Figure 7a), while the a″ vibration corresponds to the internal rotation motion (Figure 7b). Since the frequencies corresponding to these motions are small, the energy required for the formation of the complex and subsequent rotation of hydrogens to form the lower energy complex is also small. At the MP4-(SDTQ)/6-31G(d,p) level the energy difference between the two structures is 19 kcal/mol. Therefore, it is very likely that the barrier to formation of complex 4b from 4a is essentially zero and that complex 4a is either too shallow to be observed or is nonexistent. It should be pointed out that the dip in the curve of Figure 6a appears to be an artifact of the LLM path. Attempts to optimize at this point do not lead to a new stable structure.

Two similar stable ylide conformations, "bisected" (i) and "anti" (ii), were predicted by Dixon et al.[31] with anti being more stable.

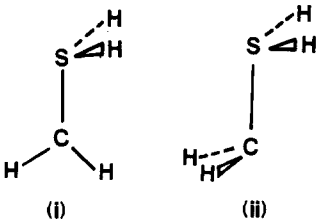

(i) (ii)

These were found by using a double ζ basis set augmented by polarization functions on the heavy atoms and a set of diffuse functions on carbon. A structure similar to bisected was obtained with our STO-2G* basis set, but with the 6-31G(d,p) basis set this structure took on the conformation 4b. The anti structure is similar to our higher energy complex 4a.

A 6-31G(d,p) LLM path connecting complex 4b with methanethiol is depicted in Figure 6b. This yields a 76 kcal/mol barrier to the formation of this complex from methanethiol. A comparison of the complex structure (Figure 4b) to that of the structures along the (C_1) IRC for reaction 7a indicates that the complex does not lie on the IRC for this reaction. A comparison of the C–S bond lengths reveals that the complex has a much shorter C–S bond (by about 0.2 Å) than any of the structures along the path.

The normal mode corresponding to the imaginary frequency of the transition state for reaction 8a is illustrated in Figure 2c. The motion suggested by this plot is that of H_2S coming off to form ethylene in one direction, while in the reverse direction the formation of ethanethiol is evident. The IRC for this reaction verifies this motion. Figure 3c shows schematics of the 6-31G(d) level IRC for this reaction.

The STO-2G* IRC for reaction 8b is represented schematically in Figure 3b. As suggested by the normal modes associated with the imaginary frequency (see Figure 2b), the structures and energies along the IRC connect smoothly with those of the separated reactants on one side and the parent molecule on the other.

Two complexes analogous to complexes 4a and 4b were found at the STO-2G* and 3-21G* levels. However, only the lower energy complex was found to exist at the higher levels of theory; attempts to optimize the higher energy structure give rise to the carbene plus H_2S fragments. The 6-31G(d,p) structure for the lower energy complex is depicted in Figure 4c. The structure is very similar to the lower energy complex between CH_2 and H_2S (Figure 4b). Comparison of this complex with the various structures along the IRC for reaction 8b shown in Figure 3b shows that the complex has a much shorter C–C bond length and C–S bond length than do any of the structures along the path.[32] Again, as for reaction 7a, the IRC for reaction 8b leads smoothly to the separated fragments at one end and the parent thiol at the other end without involving the ylide complexes.

The transition-state structure for reaction 7c is shown in Figure 1d and the normal mode corresponding to the imaginary frequency is illustrated in Figure 2d. A three-centered transition state is formed as the molecular hydrogen departs from the carbon atom. The other four atoms are very nearly coplanar. Note that the structure more closely resembles the separated products than the parent: the H–H bond is only 0.06 Å longer than that of isolated molecular hydrogen, and the C–S bond is only 0.07 Å longer than the C–S bond in CHSH.

The two four-center transition structures found for reaction 7d are shown in Figure 1, e and f, and the normal modes corresponding to the imaginary frequencies are depicted in Figure 2. The lower energy structure (Figure 2e) is similar to the transition-state structure found for reaction 7c, with the molecular hydrogen approaching the less electronegative carbon, while the higher energy structure (Figure 2f) corresponds to the hydrogens initially approaching at the sulfur end. The relative energies of these two approaches is a result of the greater electron–electron

(29) Raghavachari, K.; Chandrasekhar, J.; Gordon, M. S.; Dykema, K. J. *J. Am. Chem. Soc.* **1984**, *106*, 5853.
(30) Edmiston, E.; Ruedenberg, K. *Rev. Mod. Phys.* **1963**, *35*, 457.
(31) Dixon, D. A.; Dunning, Jr., T. H.; Eades, R. A.; Gassman, P. G. *J. Am. Chem. Soc.* **1983**, *105*, 7011.
(32) Note that, for both of the lowest energy complexes of CH_3SH and CH_3CH_2SH, the STO-2G* C–S bond length is even shorter than the 6-31G-(d,p) value and so this conclusion applies to the STO-2G* IRC.

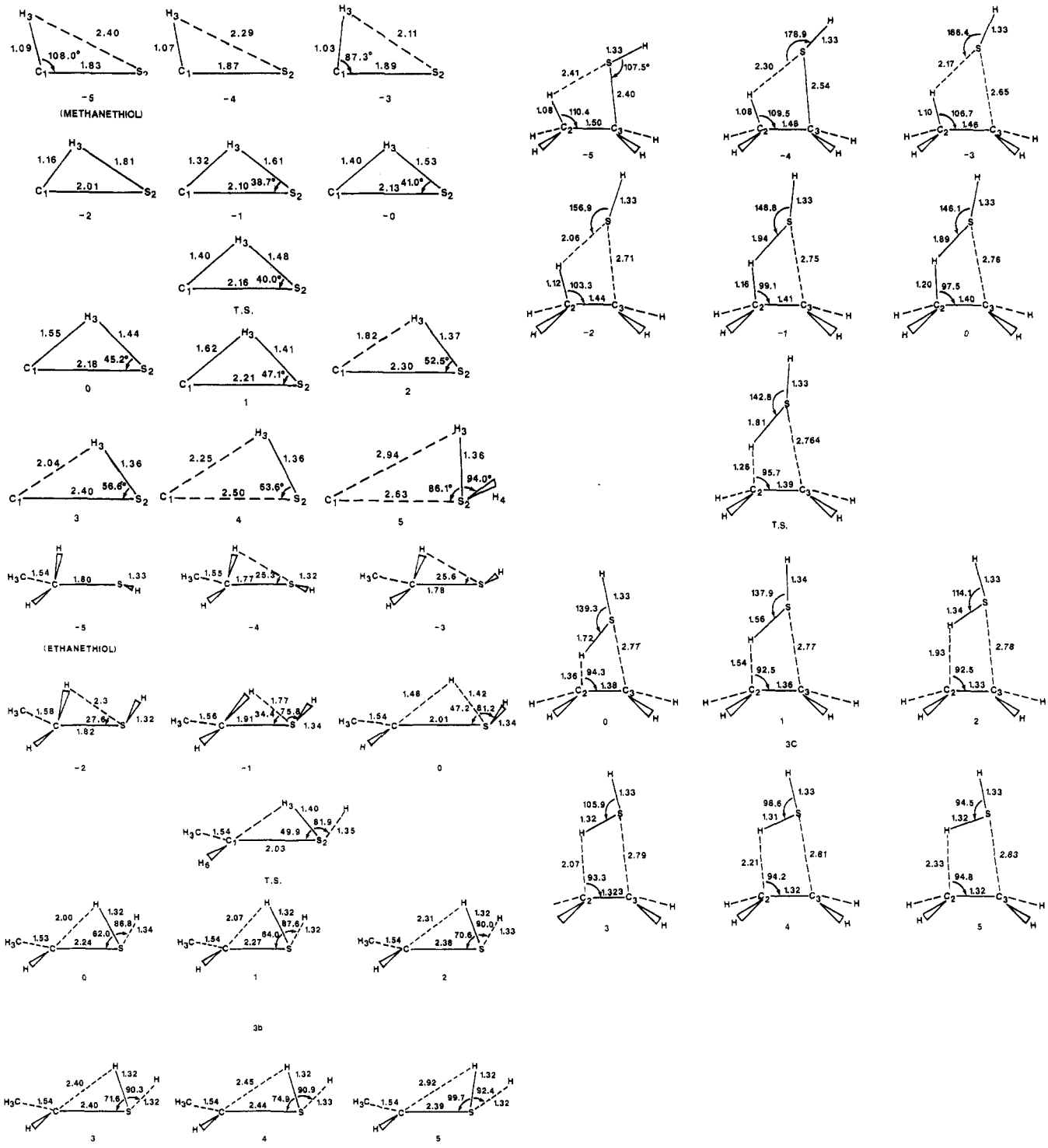

Figure 3. Schematic of structural changes along the IRC for reaction: (a) 7a, STO-2G*, (b) 8b, STO-2G*, and (c) 8a, 6-31G(d).

repulsion between the approaching H_2 and H_2CS when the approach is on the sulfur side. STO-2G* IRC's for the two approaches are illustrated in Figures 8 and 9, respectively.

B. Energetics. The energetics for reactions 7 and 8 are summarized in Table III and Figure 10. Total energies for all species considered are given in Table IV. All calculations in Table III have been carried out with the 6-31G(d,p) basis set. One can see from Table IIIb that triple excitations tend to reduce barrier heights by roughly 1 kcal/mol at the MP4/6-31G(d,p) level. There apparently is no such systematic trend for thermodynamic energy differences. As seen from Table IIIa, triples can either increase or decrease energy differences depending on the reaction; however, in general, their effect is 0–2 kcal/mol. Since MP4(SDTQ)/6-31G(d,p) calculations are rather time consuming for the molecules with three heavy atoms and since 2 kcal/mol is not likely to alter any of the conclusions drawn here, triple excitations were omitted for reactions 8.

Methanethiol Decomposition. Thermodynamically, the 1,2-molecular elimination of hydrogen to form H_2CS (reaction 7d) is the most favored pathway. However, this reaction has a high activation energy of 89.0 kcal/mol at the MP4/6-31G(d,p) level. This is more than 20 kcal/mol greater than the 67.2 kcal/mol required to break the C–S bond (reaction 7b). In fact, experimentally methanethiol is observed to decompose by a free radical mechanism.[2] The theoretical value for the C–S bond dissociation is found to be in reasonable agreement with the experimental values[14,33] ranging between 72 and 76.5 kcal/mol. The carbene

(33) Benson, S. W. *J. Am. Chem. Soc.* **1978**, *78*, 23.

TABLE IV: Total Energies (hartrees)

molecule		RHF/ 6-316**	MP2/ 6-316**	MP3/ 6-316**	MP4(SDQ)/ 6-316**	MP4(SDTQ)/ 6-316**	ZPE, kcal/mol
H_2	$D_{\infty h}$	−1.131 33	−1.157 66	−1.163 16	−1.164 56	−1.164 56	6.63
$:CH_2$	C_{2v}	−38.876 31	−38.987 10	−39.006 15	−39.010 11	−39.011 76	11.14
$^{\bullet}CH_3$	C_s	−39.564 46	−39.692 70	−39.710 18	−39.712 71	−39.714 72	19.36
C_2H_4	D_{2h}	−78.038 84	−78.316 81	−78.339 97	−78.344 12	−78.353 05	34.19
$CH_3CH_2^{\bullet}$	C_s	−78.605 53	−78.875 81	−78.904 71	−78.908 61	−78.914 82	39.50
$^{\bullet}SH$	$C_{\infty v}$	−398.068 48	−398.172 83	−398.189 92	−398.192 48	−398.194 13	4.11
H_2S	C_{2v}	−398.675 03	−398.810 03	−398.828 81	−398.831 17	−398.833 72	10.21
$:CHSH$	C_s	−436.435 44	−436.679 26	−436.704 65	−436.710 76	−436.719 73	14.67
$^{\bullet}CH_2SH$	C_1	−437.079 90	−437.327 63	−437.355 65	−437.359 89	−437.366 42	21.25
CH_3CH	C_1	−77.929 32	−78.185 33	−78.214 71	−78.219 69	−78.226 13	31.38
CH_3SH	C_s	−437.709 03	−437.987 64	−438.016 78	−438.020 61	−438.027 78	30.91
$^{\bullet}CH_2CH_2SH$	C_s	−476.114 60	−476.503 02	−476.542 09	−476.545 06	−476.547 30	40.22
H_2CS	C_{2v}	−436.509 95	−436.770 59	−436.790 66	−436.795 78	−436.806 26	16.74
CH_3CH_2SH	C_s	−476.747 40	−477.170 82	−477.210 16	−477.215 27		50.19
complex 4a	C_s	−437.559 57	−437.820 78	−437.860 11	−437.865 64	−437.872 77	26.46
complex 4b	C_s	−437.576 69	−437.863 65	−437.890 59	−437.895 06	−437.903 89	28.70
complex 4c	C_s	−476.613 81	−477.047 50	−477.083 91	−477.089 91		47.67
TS(7a)[a]	C_1	−437.523 00	−437.800 80	−437.832 90	−437.838 11	−437.846 47	25.38
TS(7c)	C_1	−437.537 95	−437.817 39	−437.847 72	−437.853 70	−437.862 64	25.08
TS(7d)[b]	C_s	−437.550 93	−437.833 50	−437.860 29	−437.864 82	−437.873 86	28.00
TS(7d)[c]	C_s	−437.473 08	−437.774 38	−437.800 02	−437.805 42	−437.816 37	24.86
TS(8b)	C_1	−476.562 52	−476.989 81	−477.030 60	−477.033 33	−477.036 97	44.94
TS(8a)	C_s	−476.608 96	−477.039 21	−477.075 47	−477.076 69	−477.083 78	44.56

[a] TS(7a) refers to the transition state for reaction 7a. [b] Lower energy transition state for reaction 7d. [c] Higher energy transition state for reaction 7d.

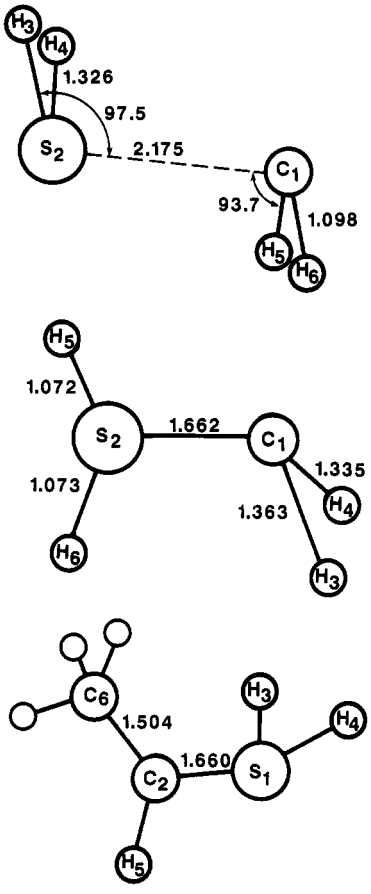

Figure 4. 6-31G(d,p) structures of stable complexes. (a) Higher energy CH_2–SH_2 *C* complex: *d*(5123) = 176.2, *d*(6124) = 176.2; ∠(516) = 94.4, ∠(512) = 97.5, ∠(321) = 93.7. (b) Lower energy CH_2–SH_2 C_1 complex: ∠(312) = 118.5, ∠(412) = 108.1, ∠(521) = 111.7, ∠(621) = 119.2; *d*(5214) = 153.0, *d*(6214) = −61.8. (c) CH_3CH_2–SH_2C_1 complex: ∠(312) = 117.5, ∠(412) = 107.1, ∠(314) = 91.2, ∠(521) = 110.3, ∠(621) = 121.4; *d*(5214) = 154.0, *d*(6214) = 120.4.

(reaction 7a) and 1,1-H_2 (reaction 7c) eliminations are both thermodynamically and kinetically unfavorable.

The formation of methylene and hydrogen sulfide has the highest activation energy, and this reaction is very endothermic

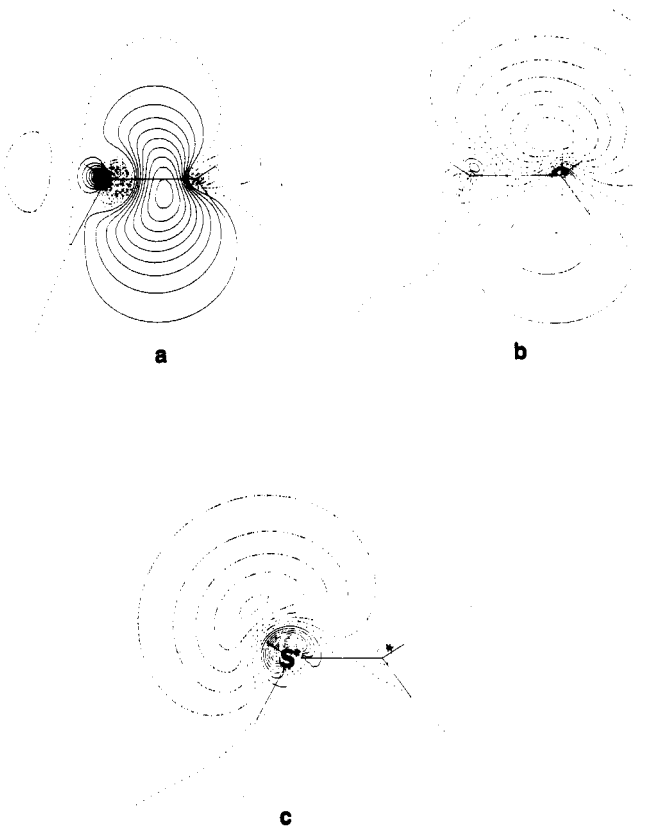

Figure 5. 6-31G(d,p) Edmiston–Ruedenberg[21] energy-localized orbitals for lower energy complex CH_2–SH_2. Contour intervals are in units of 0.05. Asterisks show atoms in the plane. The carbon is always on the right of the center. The sulfur is on the left in the center. The remaining atoms are the hydrogens. Solid lines indicate negative charge buildup, and dashed lines indicate positive charge buildup. Dotted lines show the nodal line: (a) carbon–sulfur sp orbital; (b) carbon lone pair orbital; (c) sulfur lone pair orbital.

TABLE V: Energetics for Static Pyrolysis Mechanism [6-31G(d,p)]

reaction	Δ*H*(SDQ)
(a) $CH_3CH_2SH \rightarrow CH_3CH_2 + {}^{\bullet}SH$	65.1
(b) $HS^{\bullet} + CH_3CH_2SH \rightarrow H_2S + {}^{\bullet}CH_2CH_2SH$	15.9
(c) $^{\bullet}CH_2CH_2SH \rightarrow C_2H_4 + {}^{\bullet}SH$	3.39

TABLE VI: Calculated Thermodynamic Properties and Calculated Thermodynamic Energies of Activation[a]

a. Thermodynamic Properties

	reaction	$\Delta H_0°$, kcal/mol	$\Delta_{298.15}S°$, kcal/(mol K)	$\Delta_{298.15}G°$, kcal/mol
(7a)	$CH_3SH \rightarrow :CH_2 + H_2S$	105.89 (100.895)[c]	0.0334 (0.0348)[d]	95.93 (90.52)
(7b)	$CH_3SH \rightarrow CH_3 + SH$	67.98 (72.45)	0.0310 (0.0322)[d]	58.74 (62.85)
(7c)	$CH_3SH \rightarrow :CHSH + H_2$	81.44	0.0275	73.24
(7d)	$CH_3SH \rightarrow H_2CS + H_2$	28.98	0.0268	20.99
(8a)	$C_2H_5SH \rightarrow CH_2{=}CH_2 + H_2S$	19.96 (17.23)	0.0327 (0.0309)[d]	10.21 (8.02)
(8b)	$C_2H_5SH \rightarrow :CHCH_3 + H_2S$	95.55	0.0478	81.30
(8c)	$C_2H_5SH \rightarrow CH_3CH_2 + SH$	65.84 (69.37)	0.0355 (0.0362)[d]	55.26 (58.58)
(8f)	$C_2H_5SH \rightarrow CH_3SH + :CH_2$	82.26	0.0478	68.01
(8e)	$C_2H_5SH \rightarrow :CHCH_2SH + H_2$	110.32	0.0301	101.35
(8d)	$C_2H_5SH \rightarrow CH_3CSH + H_2$	78.21	0.0298	69.33

b. Thermodynamic Energies of Activation

reaction	$E_a°$, kcal/mol	$\Delta_{298.15}S_a°$, kcal/(mol K)	$\Delta_{298.15}G_a°$, kcal/mol
$CH_3SH \rightarrow :CH_2 + H_2S$	109.42	+0.0030	108.53
$CH_3SH \rightarrow :CHSH + H_2$	99.00	−0.0004	99.12
$CH_3SH \rightarrow H_2CS + H_2$	94.36	−0.0015	94.81
$CH_2H_5SH \rightarrow CH_2{=}CH_2 + H_2S$	78.08	+0.0019	77.51
$C_2H_5SH \rightarrow :CHCH_3 + H_2S$	107.74	+0.0013	107.35

[a] Calculated by using 6-31G(d,p) scaled frequencies. [b] Calculated by using MP4(SDTQ)//6-31G(d,p) energies for reactions 7a–d and MP4(SDQ)//6-31G(d,p) energies for reactions 8a–d. [c] The singlet–triplet splitting of T_0 = 9.05 kcal/mol obtained from McKellar et al. (McKellar, A. R. W.; Bunker, P. R.; Sears, T. J.; Evenson, K. M.; Saykally, R. S.; Langhoff, S. R. *J. Chem. Phys.* **1983**, *79*, 5251) was added to the triplet ground state value from ref 18. [d] Reference 18.

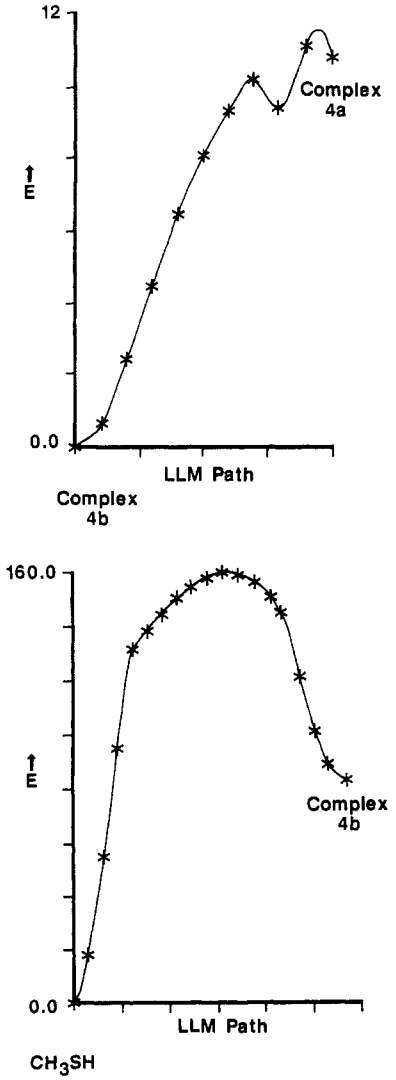

Figure 6. (a) 6-31G(d,p) SCF linear least motion path connecting complexes 4a and 4b. (b) 6-31G(d,p) SCF linear least motion path connecting complex 4b and methanethiol.

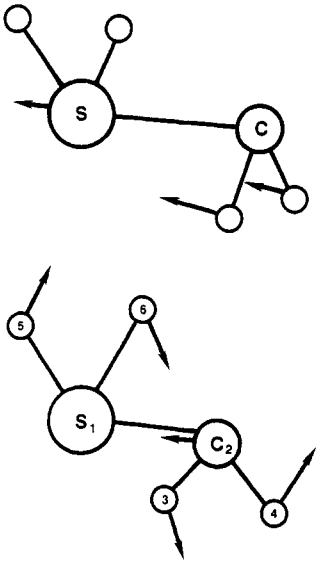

Figure 7. (a) SCF/6-31G(d,p) a′ symmetry vibration for complex 4a, frequency = 71 cm^{-1}. (b) SCF/6-31G(d,p) a″ symmetry vibration for complex 4a, frequency = 95 cm^{-1}.

(by 104.8 kcal/mol). As expected based on the Hammond postulate,[34] the transition state resembles the product structurally and energetically. This point was made earlier and is reinforced by the very small (3.5 kcal/mol) reverse activation energy for reaction 7a. Indeed, the reverse barrier for this reaction is predicted to be nonexistent at the MP4(SDTQ)/6-31G(d,p) level until zero point corrections are added. These points may be seen more graphically in Figure 10a.

The energetics of the complexes 4a and 4b with respect to methanethiol are also given in Table IIIa. Thermodynamically, complex 4b would be the more favored nondissociative rearrangement product of methanethiol on the potential energy surface by nearly 20 kcal/mol over complex 4a.

It is interesting to compare reaction 7a with the analogous reaction involving silicon:

$$H_3SiSH \leftrightarrow H_2Si + H_2S$$

The barrier to the latter reaction was calculated to be 65 kcal/mol at the MP4/6-31G(d)//RHF/6-31G(d) level of theory,[29] while that of reaction 7a was determined, in this study, to be 120.1 kcal/mol at the same level of theory. This reflects the greater

(34) Hammond, G. S. *J. Am. Chem. Soc.* **1955**, *77*, 334.

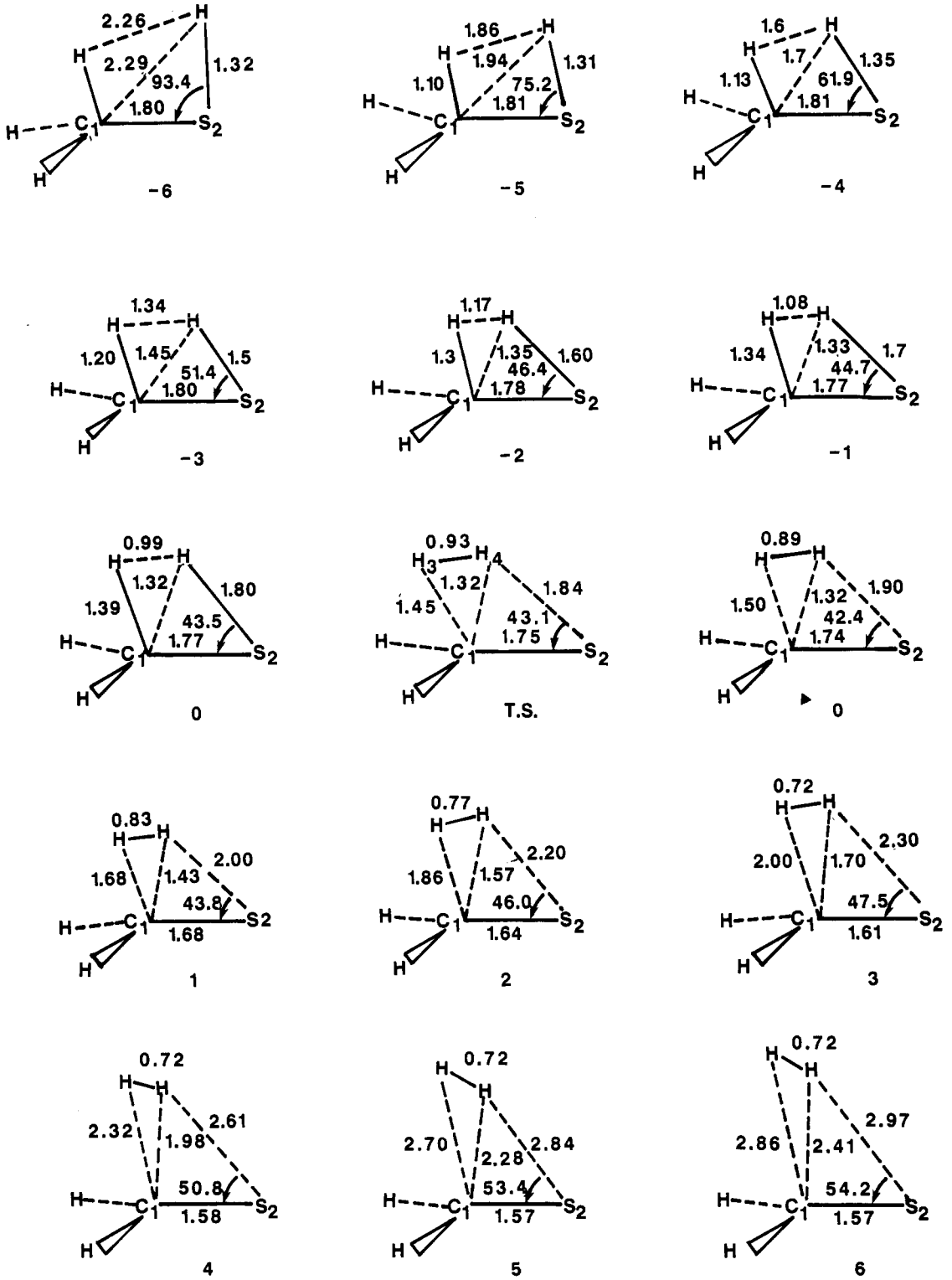

Figure 8. Schematic of structural changes along the STO-2G* $H_2CS + H_2$ IRC (approach at carbon end).

stability of silylene relative to methylene.

Reaction 7c, the 1,1-molecular elimination of H_2, is both kinetically and thermodynamically more favorable than reaction 7a, although the ΔH for the reaction is still quite large. The activation energy for the reverse reaction (insertion of :CHSH into H_2) is 17.4 kcal/mol. This is much larger than the zero barrier predicted for the reaction of CH_2 and H_2.[35]

Also illustrated in Figure 10a are the relative barrier heights for the alternative pathways for reaction 7d, the formation of thioformaldehyde. As discussed earlier in a more qualitative manner, the barrier for the approach at the sulfur end has a 27.6 kcal/mol greater activation energy than does the approach at the carbon end.

Ethanethiol Decomposition. The reaction energetics for ethanethiol are summarized in Table III and depicted graphically in Figure 10b. While the formation of ethylene and hydrogen sulfide (reaction 8a) compared to other processes is favored thermodynamically, the barrier for this reaction is greater than the energy required to break the C–S bond to form ethyl and thiyl radicals. Experimentally, ethyl mercaptan is found to decompose by two separate processes: via a bimolecular process at low temperatures and by a free radical decomposition which increases in importance at high temperatures.[2] Based on the results

(35) Sosa, C.; Schlegel, H. B. *J. Am. Chem. Soc.* **1984**, *106*, 5847, and references therein.

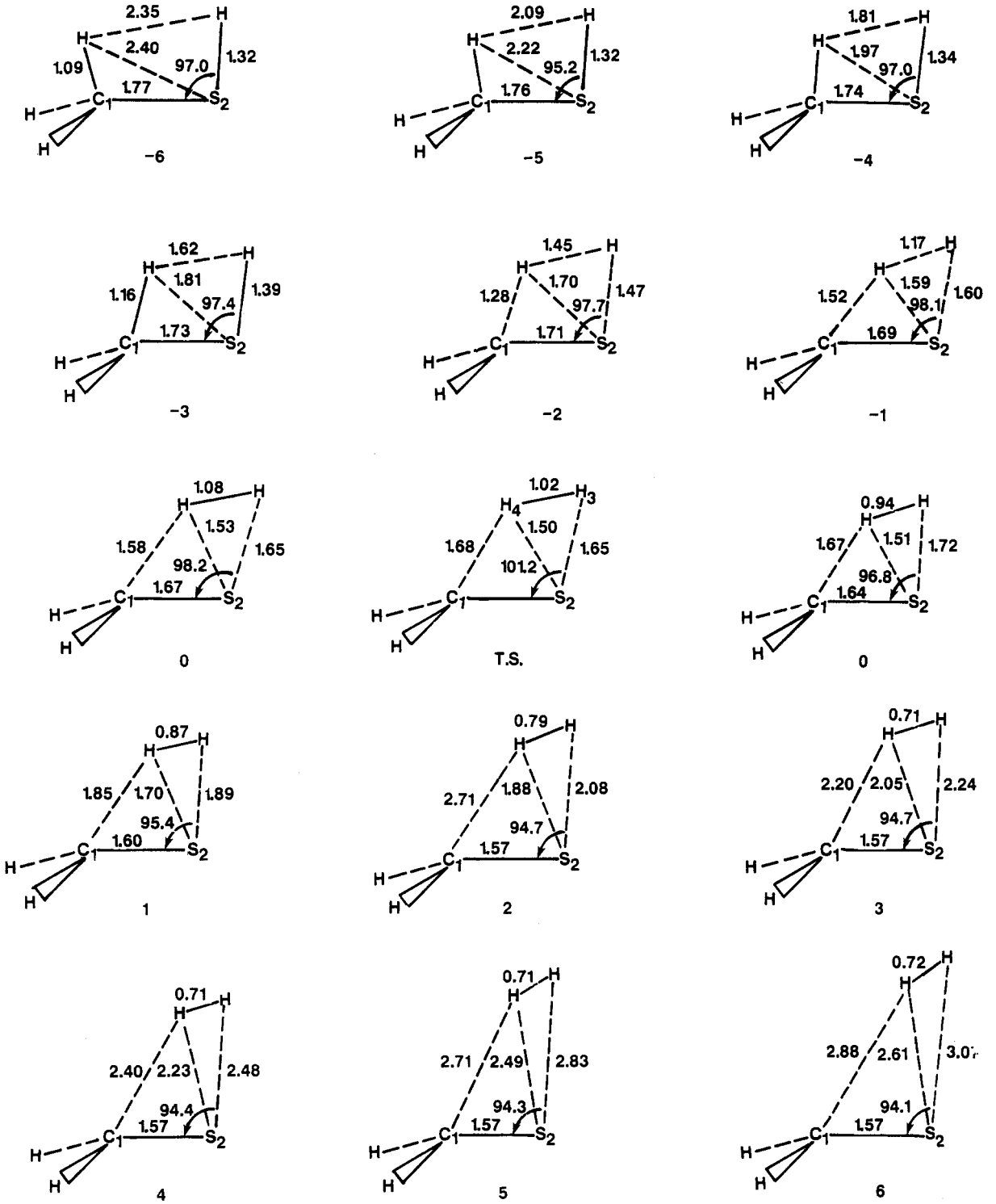

Figure 9. Schematic of structural changes along the STO-2G* $H_2CS + H_2$ IRC (approach at sulfur end).

presented here, the observed free radical process is initiated by the cleavage of the C–S bond. The value calculated for the C–S bond strength is 65.1 kcal/mol as compared with the known range of experimental values[14,33] which range from 69 to 73.5 kcal/mol. The highest energy process kinetically is the formation of CH_3CH and H_2S (reaction 8b). The carbene will presumably rearrange to its more stable isomer ethylene.[31] The energy difference between the two C_2H_4 isomers has been calculated to be 76.8 kcal/mol at the MP4(SDTQ)/6-31G(d,p)//6-31G(d,p) level, including zero point corrections. These predictions are similar to those given in a recent paper.[36]

We have considered two molecular hydrogen eliminations, reactions 8c and 8d. Of these two, reaction 8c is found to be the thermodynamically least favorable reaction considered. Reaction 8d, on the other hand, is seen to be competitive with the two radical processes. Comparing energy differences, we see that the formation of CH_3CSH and molecular hydrogen requires only about 8 kcal/mol more energy than the C–S bond cleavage, and about 7 kcal/mol less than the C–C bond breakage. However, on the basis of the results for reaction 7c presented above, there is likely to be a significant barrier to this H_2 elimination.

The static pyrolysis mechanism 8g involves three steps (Table V). The first step is a C–S bond cleavage and requires a ΔH of 65.1 kcal/mol. The second step in this mechanism, the abstraction of a hydrogen from ethanethiol by SH, requires at least

(36) Gordon, M. S.; Truong, T. N.; Pople, J. A. *Chem. Phys. Lett.*, in press.

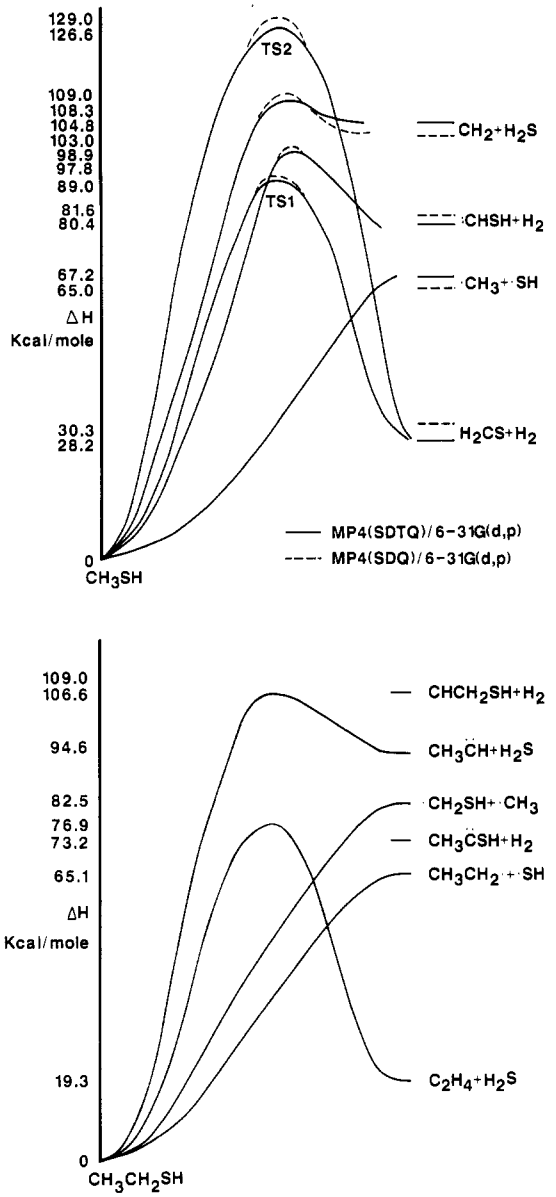

Figure 10. (a) Schematic of methanethiol potential energy surface, from MP4/6-31G(d,p) with zero point correction. (b) Schematic of ethanethiol potential energy surface, from MP4/6-31G(d,p) with zero point correction. TS1 refers to Figure 1a. TS2 refers to Figure 1e.

an additional 15.9 kcal/mol. The combined 81 kcal/mol for the first two steps is greater than the energy required for reactions 8a, 8e, or 8f to proceed thermodynamically. The overall mechanism 8g requires an additional 3.6 kcal/mol for the third step, and barriers are likely to exist for the second and third steps. Thus, it appears that the threshold dissociation process for this molecule is the homolytic cleavage of the CS bond.

Comparison with Experiment. In order to facilitate comparisons with available experimental data, the thermodynamics of the reactions investigated here have been examined in greater detail, within the rigid-rotor, harmonic oscillator approximation. Because vibrational frequencies calculated at the SCF level are generally about 10% too high,[22] the calculated frequencies have been scaled by a factor of 0.9. The resulting heats of reaction at 0 K and entropies and Gibbs' free energies at 298 K are summarized in Table VI. The trends followed by the free energies are similar to those noted above for energy and enthalpy differences, and the conclusions to be drawn from the free energies parallel those discussed earlier.

For those reactions for which experimental data are available, the calculated reaction enthalpies are within 5 kcal/mol. This is consistent with previous calculations at similar computational levels for ethane,[36] methylsilane,[37] and disilane.[38] Similar levels of agreement are obtained for the entropies and free energies. One would expect that improvement in the basis sets used (e.g., the use of triply split valence shells, more extensive sets of polarization functions, and the addition of diffuse functions) will bring the calculated values into even better agreement with experiment.[22] Similarly, basis set improvement is expected to lower most activation energies by a few kcal/mol at the MP4 level of computation.[39] It is not likely that such improvements in the wave functions will alter the qualitative conclusions drawn here, although it is possible that reaction 8a, the elimination of H_2S from ethanethiol to form ethylene directly, could become competitive with the C–S bond cleavage if the activation energy of reaction 8a is lowered by as much as 6–8 kcal/mol. A larger reduction would be required for the corresponding free energy of activation to become competitive.

Conclusions

The major conclusion in the work is that, for both methanethiol and ethanethiol decompositions, the molecular eliminations are unfavorable relative to the other pathways, because the barriers to these eliminations are rather high. Apparently in agreement with experiment for both decompositions, radical processes involving the C–S bond cleavage are predicted to be the most favored energetically. Thus, one would predict that the mechanism for pyrolysis of thiols would involve a radical process rather than the proposed molecular processes. However, the elimination of H_2S from ethanethiol to form ethylene directly could become competitive with the C–S bond cleavage if computational improvements decrease the activation energy of reaction 8a by as much as 6–8 kcal/mol. Of the two forms of bond cleavage proposed, C–S (reactions 1 and 2) or C–C (reaction 6a), one would probably expect C–S cleavage to occur more favorably since this would break the weaker of the two bonds considered.

Recent experiments[10] suggest that vacuum pyrolyses of highly strained thiol systems result in the formation of carbenes as an important primary product. Theoretical and experimental investigations of the molecular features responsible for carbene formation are under investigation.

Acknowledgment. This work was supported by grants from the Petroleum Research Fund, administered by the American Chemical Society, and the National Science Foundation (No. CHE83-09948). The computer time used in the calculations was provided by the North Dakota State University Computer Center.

Registry No. CH_3SH, 74-93-1; CH_3CH_2SH, 75-08-1.

(37) Truong, T. N.; Gordon, M. S., manuscript in preparation.
(38) Gordon, M. S.; Truong, T. N., Bonderson, E. K. *J. Am. Chem. Soc.* **1986**, *108*, 1421.
(39) Gordon, M. S.; Gano, D. R.; Binkley, J. S.; Frisch, M. J. *J. Am. Chem. Soc.* **1986**, *108*, 2191.